Layman's summary

The Circle of Willis (CoW) is a structure of arteries that supply blood to the brain. Abnormalities in this system can cause a series of cerebrovascular diseases, including unruptured intracranial aneurysms (UIAs). UIAs are caused by the weakening of a wall of an artery, which expands in volume. This can lead to rupture (subarachnoid hemorrhage, SAH), which causes death in over 35% of cases and leaves most of the survivors with long-term disability.

In cases of aneurysms with a diameter above 5 mm, the abnormality can be surgically treated. This risky procedure, however, is linked with poor neurological outcomes in 6-10% of cases. Frequently, smaller aneurysms are left untreated because the risk of preventive repair does not outweigh the risk of spontaneous rupture, and are monitored through imaging (e.g. TOF-MRA or CTA). Diagnosis is possible through imaging, but its accuracy might depend on many factors including quality of the MRA, level of experience, size and position of the aneurysm. In fact, in up to 10% of cases, UIAs are missed during screening, especially for small aneurysms. For this reason, an automatic atlas-based method of at-risk-areas and aneurysm detection is proposed.

The atlases, based on the TOF-MRAs of 544 healthy adults, can address the high variability in the anatomy of the CoW, differences in age and types of scanner. This pipeline uses 4 statistical atlases and a TOF-MRA from a patient. The patient image gets preprocessed, its CoW is segmented, and the radius of the resulting vessels is calculated (radius map). Then, the preprocessed atlases are registered to the preprocessed TOF-MRA. Lastly, the registered atlases and radius map are used to calculate the Z-score map. The Z-score maps are represented as 3D colour-coded maps superimposed on the TOF MRA image. They are used as a way to highlight areas on the CoW that significantly diverge from the healthy anatomy.

In this study, Z-score maps from 19 patients and 18 healthy subjects are compared. Moreover, two types of binary masks are evaluated: the manually segmented aneurysm mask provided with the patient data and a binary 3D sphere of fixed radius. From the analysis of the two binary masks, we concluded that the sphere, with its larger volume, performs better in terms of aneurysm detection. This finding could prove useful because it would be a quicker solution compared to labor-intensive and time-consuming manual segmentation. From the comparison between patients and healthy images, we see that this method is able to detect the difference between an image containing an abnormality and one that does not. This could serve as a quick way to sort through large amounts of unlabeled images. More importantly, this pipeline is able to correctly detect the aneurysm in the image in 16 cases out of 19 (sensitivity 84%) using the aneurysm binary mask, and 17 cases out of 19 (sensitivity 89%) using the sphere.

In conclusion, this color-coded map can be used to assist clinicians in focusing their attention on areas that are at risk of developing an aneurysm or the aneurysm itself. It could also be useful in research, being able to quickly sort large amounts of unlabeled data, or in concomitance or support of segmentation techniques.

Investigation of cerebral vascular abnormalities in TOF-MRA brain images

Author: Giulia De Donno
First reviewer: Dr. H. Kuijf
Second reviewer: Dr. ir. K. Vincken
Daily supervisor: K. M. Timmins

ABSTRACT

Abnormalities in the arterial system can lead to a series of cerebrovascular diseases including unruptured intracranial aneurysms (UIAs). UIAs are present in around 3% of the population, and upon rupture, 35% of cases result in death and most of the survivors are left with long-term disabilities. Aneurysms are usually small in size and vary greatly in shape and position in the vessel configuration. It is one of the reasons why up to 10% of UIAs are missed during screening. For this reason, in this study, an automatic atlas-based method of at-risk-areas and aneurysm detection is presented. The pipeline outputs a color-coded map that can be superimposed on the TOF-MRA image, indicating areas that diverge from the average healthy anatomy in the form of Z-scores. High Z-scores are potentially linked to the presence of abnormalities. This method was tested on 19 TOF-MRA containing one aneurysm above 5 mm in radius and 18 images with healthy anatomy. After preprocessing, the TOF-MRA underwent vessel segmentation and vessel radius calculation. The resulting image, as well as the preprocessed atlases registered to the patient's space, are then used to calculate the Z-score maps. Using two different types of segmentation for evaluation, aneurysms were detected in up to 17 images out of 19. An analysis of the Z-scores in areas outside the segmentations showed no statistical differences compared to the Z-score map from healthy subjects. This method has the potential to be useful in a clinical setting, as well as research, as part of larger projects.

Keywords: Unruptured Intracranial Aneurysm (UIA); Aneurysm detection; Z-score; TOF-MRA; Atlas; Vessel abnormalities

1. Introduction

When the wall of an artery is weakened it can expand creating an aneurysm, commonly found in the Circle of Willis (CoW). Up 3% of the population presents unruptured intracranial aneurysms (UIAs), with a strong prevalence of cases in first- and second-degree relatives of patients (around 20%).[1,2] This type of degenerative disorder can be influenced by a combination of genetic, idiopathic and environmental risk factors, yet it is still unclear how those factors contribute to the development of aneurysms.[3,1,4]

The rupture of an aneurysm leads to subarachnoid hemorrhage (SAH), which results in death in 35% of cases, and leaves most of the survivors with long-term disability.[5] An accurate and early diagnosis is important since preventive therapy has been associated with more favorable clinical outcomes, lowering the risk of death and disability caused by rupture.[6]

Surgical clipping or endovascular treatments can be used to preventively repair the aneurysm. These procedures, however, are linked with poor neurological outcomes in 6-10% of cases, which in many cases is higher than the risk of rupture itself. Frequently, small aneurysms (<5 mm in diameter) are left untreated because the risk of preventive repair does not outweigh the risk of spontaneous rupture. In this case, imaging (e.g. TOF-MRA or CTA) is used to monitor the dimension of the aneurysm over time.[3] To this end, three-dimensional time-of-flight magnetic resonance angiography (3D TOF-MRA) is often used, being a non-invasive method to image the blood flow within the vessels in the brain.[6]

Often aneurysms are incidentally detected while investigating other non-specific symptoms (e.g. headache and vertigo) since aneurysms rarely present symptoms before rupture.[3] Radiologists can diagnose aneurysms from TOF-MRAs, however, their diagnostic accuracy depends on many factors, including quality of the MRA, level of experience, size and position of the aneurysm.[7] In fact, in up to 10% of cases UIAs are missed during screening, especially small aneurysms.[8]

Furthermore, abnormalities in the arterial system are the cause of many cerebrovascular diseases, such as stroke (ischemic and hemorrhagic), arteriovenous malformations, white matter hyper-intensities and atherosclerosis. [9–12]

For this reason, an automatic or semi-automatic tool to detect cerebrovascular abnormalities and aneurysms could prove diagnostically useful. Moreover, typically research screening studies for patients with a high risk of UIAs involve a large volume of TOF-MRA images, and an automatic tool would allow researchers to analyze the data faster and more accurately.

Due to the high complexity of this issue, many different types of (semi-) automatic UIA detection methods have been developed. Some semi-automatic methods are mostly based on the shape of the aneurysm, other automatic techniques rely on deep learning. These types of detection can be voxel-based or surface-based, for example using vessel surface meshes.[8,13]

In this report, an automatic atlas-based method of at-risk-areas and aneurysm detection is described. As a way to address the high variability in the anatomy of the Circle of Willis[11] (CoW), age and different protocols and scanners used, four types of statistical cerebroarterial atlases based on healthy patients are employed.[9] These statistical cerebroarterial atlases are based on the TOF-MRA of 544 healthy adults, and they represent morphology and distribution of the artery system in the form of mean intensity in the TOF-MRA, artery radius and its standard deviation and artery probability. From the combination of the atlases and the TOF-MRA images from patients, a 3D map of coefficients (Z-score) has been calculated and used as a way to highlight areas on the CoW that significantly diverge from the healthy anatomy. The output is shown as a colour map overlaid on the TOF MRA image, and it is evaluated through visual examination and statistical analyses.

2. Materials and Methods

2.1 Data

2.1.1 Statistical Atlases

The statistical atlases of cerebral arteries used have been created by Mouches and Forkert[9]. They are based on 544 TOF-MRA and T1-weighted images from healthy subjects. The images are acquired at different centres and scanners, from individuals with an age range of 19-86 years (mean: 47 years), with a slight prevalence of males (54%). The atlases have an isotropic voxel dimension of 0.5 mm^3. A brief description of the atlases is presented below, more details can be found in the original paper[9].

1. **TOF MRA average atlas** (intensity atlas). Each voxel represents the mean of the intensity of the corresponding voxel in all the 3D images.
2. **Artery probability atlas** (probability atlas). It is the average of the artery segmentations from all patients. Each voxel represents the probability between 0 and 100 for a voxel to be part of an artery.
3. **Mean artery radius map** (radius atlas). Represents the mean radius in each voxel.
4. **Standard deviation map** (STD atlas). Represents the standard deviation of the artery radius for each voxel.

2.1.2 Dataset

The dataset used in this study is a subset of the data released as part of the ADAM challenge for MICCAI 2020[8]. From the 113 cases in the released training dataset, a subset was made of patients presenting one aneurysm of at least 5 mm of radius (n= 20, patient dataset) and 18 images without aneurysms were used as controls for comparison (healthy dataset). A patient case consisted of a bias-corrected TOF-MRA image, a binary mask of the aneurysm, and a file containing the voxel coordinate of the center of mass of the aneurysm and the radius for all unruptured and untreated aneurysms. Other files available were not used in this study.

2.2 Methods

A schematic description of the pipeline can be found in Figure 1.

2.2.1 Preprocessing

The TOF-MRAs and the four atlases (as described in sections 2.1.1 and 2.1.2) were resampled to the mean voxel size of the images in the dataset (0.357, 0.357, 0.500) mm. The intensity values of the TOF-MRA and intensity atlas were normalized between the 5th and 95th percentile (histogram correction). Before resampling, the aneurysm segmentation was thresholded, keeping only values of 1 (untreated aneurysm) (Figure 1.a).

Firstly, an existing, trained CNN model with 3D U-Net architecture[10] was used to perform cerebral vessel segmentation from the pre-processed TOF-MRA images. The main vessels (including the Circle of Willis), were then selected from the extracted vessels segmentation using connected component analysis (3D-26 neighborhood, minimum cluster size 1000 voxel) using MeVisLab (MeVis Medical Solutions AG, Bremen, Germany). The performance of the segmentation CNN was already evaluated in previous studies[10,13] and each segmentation was visually checked. Due to the large anatomical

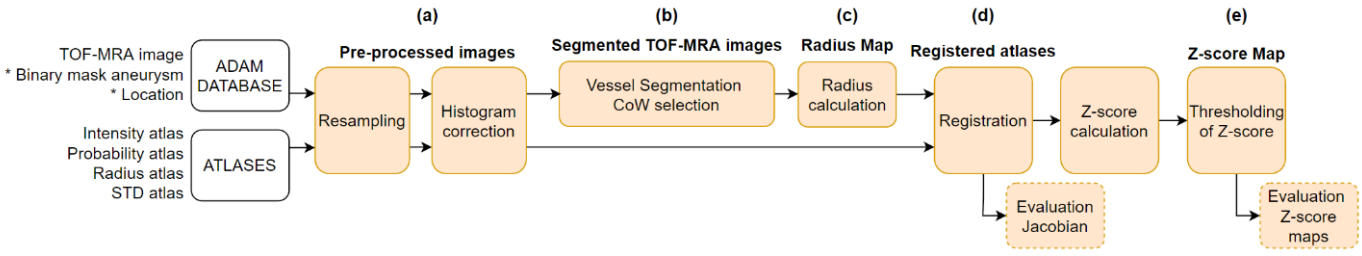

Figure 1. *Representation of the pipeline used to calculate the Z-score maps for both the patient and healthy dataset. (*) not used for healthy dataset.*

variability of the CoW, a more conservative approach regarding the inclusion of vessels allowed a larger amount of branches to be included (Figure 1.b).

Secondly, after vessel segmentation and removal of small unconnected components, the Danielsson[14] radius of the vessels was determined. This algorithm was chosen as it was the same as was performed by Mouches[9] to create the radius atlas. In order to do that, from the segmented image two images were created with opposite values of background and foreground (0,1). From the image with a positive foreground, skeletonisation was used to extract the centerline and added to the image with a positive background. The resulting image was used to calculate the Danielsson radius map (Figure 1.c).

Lastly, to generate a Z-score of the patient radius map relative to the atlas, it was important that all images were registered to each other (Figure 1.d).

Firstly, for each TOF-MRA, the intensity atlas was registered to the image using affine and B-spline (see appendix for parameter files). Using the resulting registration parameters, the other three atlases (radius, standard deviation and probability) were then transformed to the same space as the patient TOF-MRA (with final B-spline value = 1), and the Jacobian map was calculated.

The registration of the atlases to the patient's space was evaluated ensuring that the resulting atlases maintained intensity values in the correct range (intensity atlas: [0-1], mean radius atlas: [0-4], probability atlas: [0-100], standard deviation atlas: [0-1.3]). The Jacobian map was carefully examined to ensure the absence of foldings of large dimensions, especially if those areas would overlap with the CoW in the registered image. In that case, the registration was assumed inadequate and the TOF-MRA was excluded from further analysis (excluded n =1). For further information about the Jacobian, we refer to the Elastix Manual[15].

2.2.2 Z-score Map Generation

The Z-score is a standardized parameter that quantifies how much a new observation diverges from the normative average. If the Z-score is 0, the observation is identical to the mean score, if it is 1 indicates that that observation is greater than the mean value and diverges from it by 1 standard deviation and so on.

The Z-score of the radius map x was determined relative to the registered radius atlas μ and standard deviation atlas σ to generate a patient Z-score map.[9] In the patient radius image, the Z-score was calculated for each voxel, i (Eq. 1, Figure 1.e).

$$Z_i = \frac{x_i - \mu_i}{\sigma_i} \qquad (Eq.\,1)$$

The resulting patient z-score map was masked using the registered probability atlas (threshold 0.1) to reduce noise and remove detections outside the vessels. For future steps, we only focus on positive Z-scores due to the nature of the abnormalities that we want to detect.

2.3 Evaluation

In the development of the pipeline, a visual evaluation was performed at each step. Color Z-score maps were made of the vessels, where higher Z-scores could indicate abnormalities and aid radiologists in cerebrovascular assessment (Figure 3.a).

Figure 2 summarizes the experiments performed to evaluate the Z-score map and its ability to detect abnormalities (especially aneurysms). For each image within a certain category, mean, standard deviation and percentiles (25th, 50th, 75th, 95th, 99th, and 100th) have been calculated for non-zeros values

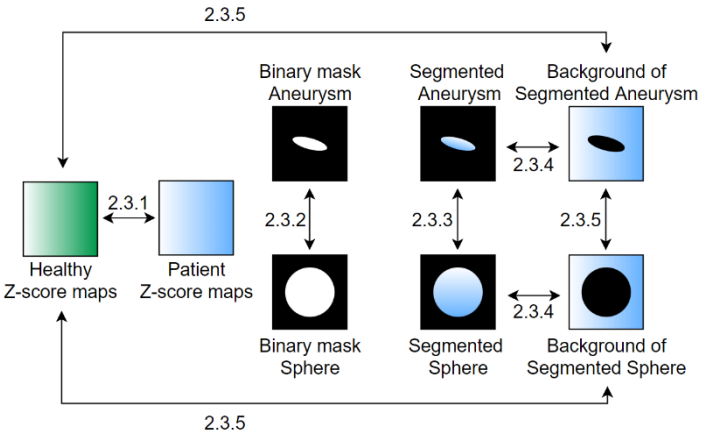

Figure 2. *Schematic representation of the evaluation strategy used to assess the aneurysm detection performance in the Circle of Willis.*

in the Z-score maps. These types of information have then been represented graphically.

2.3.1 Patient and healthy dataset

Firstly, an overall analysis of the patient and the healthy dataset was provided (Figure 2, 2.3.1). For each full Z-score map in both datasets, the mean, standard deviation and percentiles of Z-scores were determined. Then the two sets of percentiles in the healthy and patient groups were compared using one-way ANOVA to test for statistically significant differences ($p < 0.05$).

2.3.2 Binary mask: Aneurysm and Sphere

For the analysis of the Z-score maps on the patient images, two types of aneurysm segmentation have been used. The first is a binary mask of the aneurysm, a voxel-wise segmentation provided with the dataset. The second aneurysm segmentation is a binary 3D sphere centered in the center of mass of the aneurysm, with the radius of the largest radius (in mm) found in the text file provided in the dataset.

An analysis of the two types of masks has been conducted, comparing volumes and amount of non-zero Z-scores found within their boundaries (Figure 2, 2.3.2).

2.3.3 Segmented Aneurysm and Sphere

In this section, the Z-scores contained in the binary segmentations are evaluated (Figure 2, 2.3.3). For each image, a comparison (one-way ANOVA, $p < 0.05$), between the segmented aneurysm and sphere is performed. The aim is to detect which segmentation type performs better in aneurysm detection.

2.3.4 Segmentations and Backgrounds

We define as background the Z-scores maps with the segmentation aneurysm or sphere removed. To assess aneurysm detection performance, an analysis comparing the Z-scores within the segmented areas and their background is performed (Figure 2, 2.3.4). If the area within the segmentation had a statistically different value from the background ($p < 0.05$, one-way ANOVA test), it was considered true positive detection of an aneurysm. Sensitivity was calculated as the total number of true positives divided by the total number of aneurysms (number of images) in the patient dataset. This analysis was performed for both the aneurysm and the sphere segmentation.

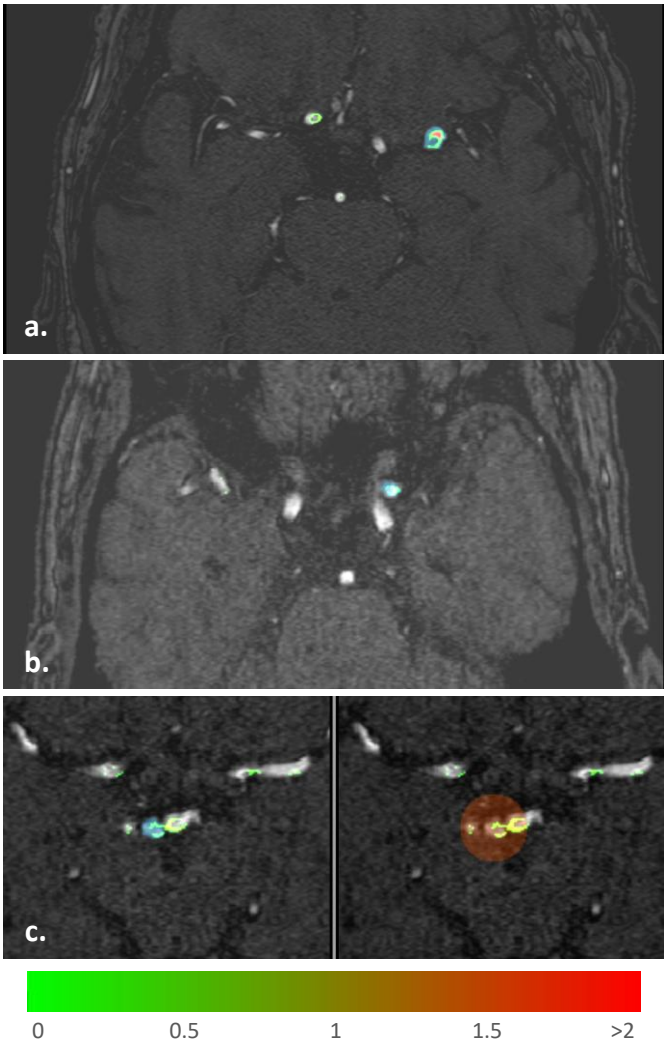

Figure 3.a *Example of Z-score map for a successful detection. In this case, the aneurysm binary mask is shown (light blue). The green color indicates a low value Z-score, the red a higher one. We can see how other potential abnormalities are detected in the background.*

Figure 3.b *Example of an unsuccessful detection. The Z-scores detected have low values, not significantly different to the background.*

Figure 3.c *For the same patient, we see on the left a representation of an unsuccessful detection of the aneurysm using the aneurysm binary mask; on the right, its successful detection using the sphere.*

2.3.5 Backgrounds and healthy dataset

With the backgrounds defined in section 2.3.4 for both aneurysm and sphere segmentation, two types of analysis have been performed (Figure 2, 2.3.5).

The first comparison was between Z-scores from the backgrounds of the aneurysm and sphere for each image. The second was made between the percentiles of the two types of backgrounds and the healthy database (p 0,05, one-way ANOVA in both cases). The aim is to understand if the Z-scores in the background of images from patients have substantial differences from the ones in healthy subjects.

3. Results

3.1 Patient and healthy dataset

The 19 images from the patient dataset had one aneurysm with a mean radius of 6.1 ± 0.6 mm (range: 5.12 and 7.12 mm). From these, the Z-score maps produced had Z-scores in the range 0.00 - 4.84 (mean maximum value 2.6 ± 0.85), whereas the healthy dataset varied within the range of 0.00 - 3.09 with a mean maximum value of 2.03 ± 0.66.

Figure 4 illustrates the percentiles of Z-scores from the patient and healthy dataset. The differences between every Z-score percentile from the two groups found to be was statistically significant ($p < 0.05$, ANOVA one-way test).

3.2 Binary mask: Aneurysm and Sphere

As described in section 2.3.2, two types of segmentation have been used to evaluate this pipeline (Figure 2, 2.3.2). The sphere had a radius of 7.12 mm for all images. Its volume was between 2 and 10 times the volume of the aneurysm segmentation (mean value 4.4 ± 2.4) and incorporated it entirely. As expected, the sphere contained more voxels with positive Z-scores compared to the aneurysm, more specifically between 1.02 and 23.50 times (3.62 ± 6.53), representing 4.3 ± 2.4% and 18.8 ± 9.4% of the volume of the sphere and segmented aneurysm. An example can be visualized in Figure 3.c.

3.3 Segmented Aneurysm and Sphere

In this section, the Z-scores in the segmented aneurysm and sphere were compared for each image (Figure 2, 2.3.3). As previously mentioned, the two segmentations contained a different amount of positive Z-scores. Nonetheless, significant differences ($p < 0.05$, ANOVA) have been found only in 4 images out of 19. By visual inspection of the images, a cluster of higher Z-scores was usually found mostly in the sphere, and only partially in the aneurysm segmentation (Figure 3.c). As we can see in Figure 5, the segmented aneurysms (A) tend to have a slightly lower mean Z-score but a higher standard deviation compared to the sphere (S).

3.4 Segmentations and Backgrounds

In this section, as described in section 2.3.4, the Z-score map of the segmented areas has been compared to their relative background (Figure 2, 2.3.4). Only 2 images did not present statistically significant differences ($p < 0.05$, ANOVA test) for both pairs of segmentation and background. This means that the aneurysm was not detected, therefore we consider this a false negative detection (Figure 3.b).

In one case, however, a significant difference was found for the sphere segmentation, but not for the

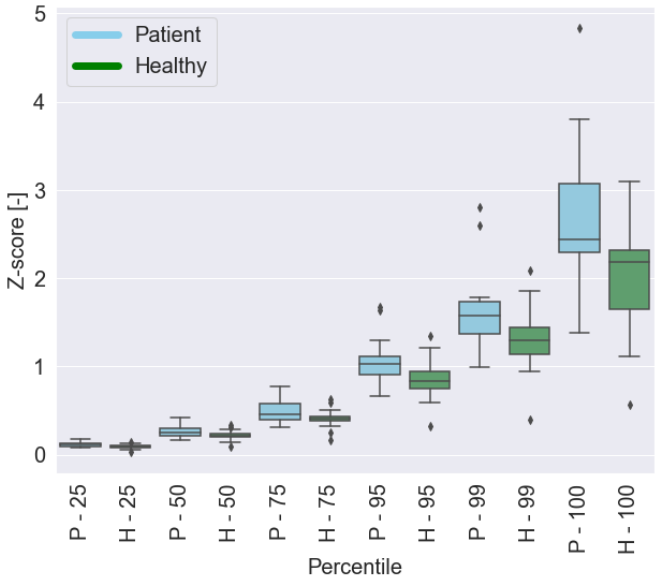

Figure 4. *Comparison between the percentiles of the non-zero Z-scores from each image between the patient dataset (P) and the healthy dataset (H).*

aneurysm. The aneurysm detection sensitivity for each type of segmentation is 84% for the aneurysm and 89% for the sphere.

3.5 Backgrounds and healthy dataset

From the comparison image by image between the background of the sphere and the background of the aneurysm, only in 2 images a significant different ($p < 0.05$, ANOVA test) was found.

The calculation of statistical differences between the Z-scores percentiles of healthy group, aneurysm backgrounds and sphere backgrounds did not show any statistical difference for each combination of the three groups (Figure 2, 2.3.5)

4. Discussion

In this paper, an automatic atlas-based method of at-risk-areas and aneurysm detection is presented. This method, based on the use of atlases from healthy subjects, can output a colour-coded Z-score map in a few minutes, requiring minimal interaction from the operator. This study showed that images containing an abnormality result in Z-score maps that are significantly different compared to the ones that do not. This characteristic could prove useful as a way to flag in advance images that might present some sort of abnormalities, especially in a large dataset of images. The presence of aneurysms is linked with higher Z-scores, and this pipeline was able to correctly identify their presence in 84% and 89% of images, depending on the type of segmentation used.

In their study, Mouches and Forkert[9] indicated how even healthy individuals could present high Z-scores (absolute values above 2) due to different anatomy and, for this reason, a number of healthy subjects have been included in this study for comparison. It is important to highlight that instead of absolute values, only positive Z-scores have been analyzed due to the origin of the abnormality that we are trying to detect (vessels whose radius exceeds the population average).

This study proved that Z-score maps from healthy subjects present significant differences compared to the ones from patients, and that these differences are

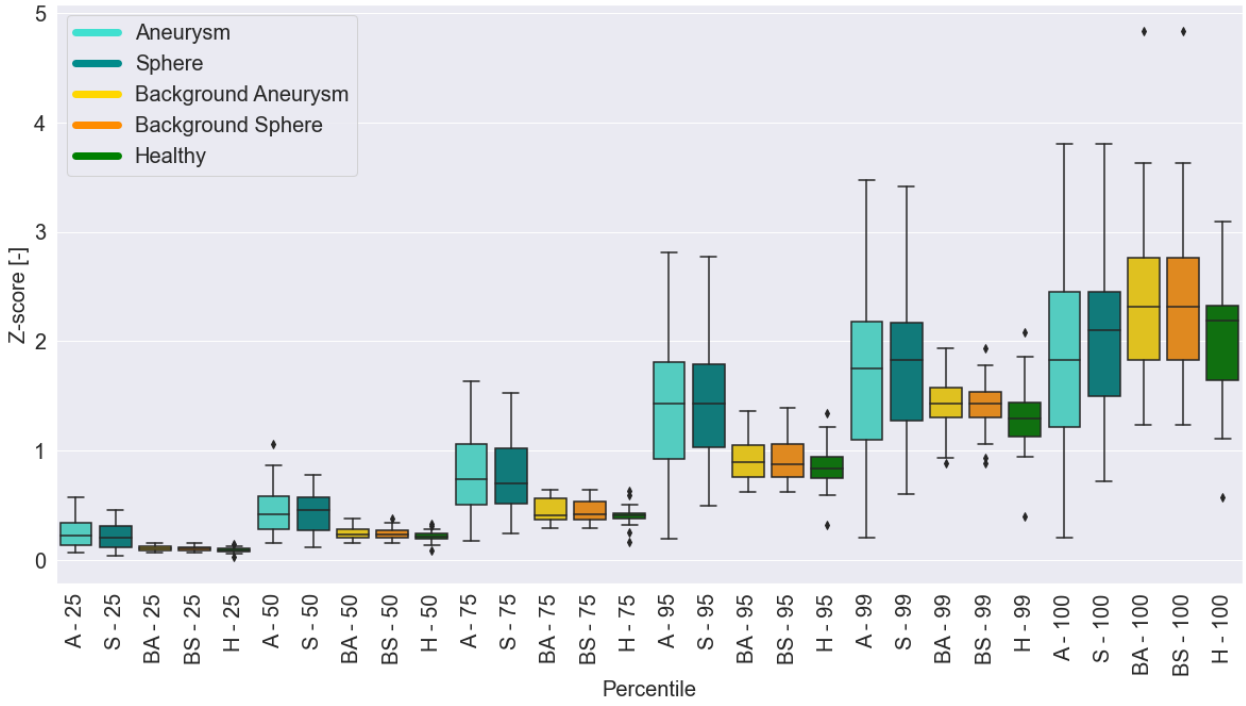

Figure 5. *Visual comparison of the percentiles of the Z-scores of each image in each category: aneurysm segmentations (A), sphere segmentations (B), backgrounds of aneurysm (BA), backgrounds of sphere (BS), as defined in section 2.3.4, and images from the healthy database.*

due to the presence of the aneurysm. This indicates that even if small abnormalities are found in the background of the segmented images, their magnitude is not high enough to be flagged as an aneurysm.

Only in two images the segmented areas and the backgrounds did not present a significant difference, and we can consider that as a false negative detection. A possible reason could be some registration or segmentation issue (Figure 3.b).

Due to the need for an experienced professional to perform aneurysm segmentation and the time-consuming nature of this process, we demonstrate the use of a sphere segmentation. The sphere proved to work slightly better compared to the binary segmentation provided, being able to better include abnormalities found in the proximity of the aneurysm segmentations, but not entirely within it. This could be caused by a slight misalign between the TOF-MRA image and binary mask due to resampling and registration, or issues during segmentation or registrations.

4.1 Limitation to the study

In this study, only 19 images from the patient database and 18 from the healthy database have been compared, and a larger sample size would bring a stronger statistical power. Moreover, relatively large aneurysms have been analysed, in which the Z-score maps reached higher values. For smaller abnormalities or aneurysms, smaller Z-scores have to be expected. This could make the detection of aneurysms of small size more difficult. It is to be questioned, however, if the use of atlases can represent well all degrees of anatomical variability of the CoW. Lastly, including a clinician's expertise in the analysis of the background of the images would have been beneficial. In this way, it would have been possible to discern if high Z-scores clusters in the images are indeed linked to abnormalities, areas at risk of developing aneurysms, or just noise.

4.2 Future work

The current pipeline is only able to detect the presence of the aneurysm in the image, but not its coordinates. A way to automatically detect significant clusters of high Z-scores and define their position could be a useful addition to the pipeline. Furthermore, once the algorithm is developed, it would be possible to rank abnormalities by risk category, adding more information to the color-coded map. Additionally, it would be interesting to see how the pipeline performs with smaller aneurysms and with the presence of more than one aneurysm.

5. Conclusion

This pipeline is able to create a color-coded map indicating areas in the brain that diverge from the average healthy anatomy. This only requires a TOF-MRA image and the 4 statistical atlases, and minimal interaction from the operator. This color-coded map, which can be superimposed on the TOF-MRA image, could be used to assist clinicians in focusing their attention on small areas at risk of developing an aneurysm, or the presence of the aneurysm itself. Moreover, it can be useful for the researcher to sort large amounts of data, or in concomitance to other segmentation or detection techniques.

In conclusion, this pipeline can be used to discern between healthy and patient data, and accurately detect the presence of aneurysms in up to 89% of images.

6. References

(1) Brown, R. D.; Huston, J.; Hornung, R.; DR.P.H; Foroud, T.; Kallmes, D. F.; Kleindorfer, D.; Meissner, I.; Woo, D.; Sauerbeck, L.; Broderick, J. Screening for Brain Aneurysm in the Familial Intracranial Aneurysm Study: Frequency and Predictors of Lesion Detection. *Journal of Neurosurgery* **2008**, *108* (6), 1132–1138. https://doi.org/10.3171/JNS/2008/108/6/1132.

(2) Vlak, M. H.; Algra, A.; Brandenburg, R.; Rinkel, G. J. Prevalence of Unruptured Intracranial Aneurysms, with Emphasis on Sex, Age, Comorbidity, Country, and Time Period: A Systematic Review and Meta-Analysis. *The Lancet Neurology* **2011**, *10* (7), 626–636. https://doi.org/10.1016/S1474-4422(11)70109-0.

(3) Hackenberg, K. A. M.; Hänggi, D.; Etminan, N. Unruptured Intracranial Aneurysms. **2020**, 8.

(4) Bor, A. S. E.; Velthuis, B. K. Configuration of Intracranial Arteries and Development of Aneurysms. **2008**, 7.

(5) Nieuwkamp, D. J.; Setz, L. E.; Algra, A.; Linn, F. H.; de Rooij, N. K.; Rinkel, G. J. Changes in Case Fatality of Aneurysmal Subarachnoid Haemorrhage over Time, According to Age, Sex, and Region: A Meta-Analysis. *The Lancet Neurology* **2009**, *8* (7), 635–642. https://doi.org/10.1016/S1474-4422(09)70126-7.

(6) HaiFeng, L.; YongSheng, X.; YangQin, X.; Yu, D.; ShuaiWen, W.; XingRu, L.; JunQiang, L. Diagnostic Value of 3D Time-of-Flight Magnetic Resonance Angiography for Detecting Intracranial Aneurysm: A Meta-Analysis. *Neuroradiology* **2017**, *59* (11), 1083–1092. https://doi.org/10.1007/s00234-017-1905-0.

(7) Alwalid, O.; Long, X.; Xie, M.; Han, P. Artificial Intelligence Applications in Intracranial Aneurysm: Achievements, Challenges and Opportunities. *Academic Radiology* **2022**, *29*, S201–S214. https://doi.org/10.1016/j.acra.2021.06.013.

(8) Timmins, K. M.; van der Schaaf, I. C.; Bennink, E.; Ruigrok, Y. M.; An, X.; Baumgartner, M.; Bourdon, P.; De Feo, R.; Di Noto, T.; Dubost, F.; others. Comparing Methods of Detecting and Segmenting Unruptured Intracranial Aneurysms on TOF-MRAS: The ADAM Challenge. *Neuroimage* **2021**, *238*, 118216.

(9) Mouches, P.; Forkert, N. D. A Statistical Atlas of Cerebral Arteries Generated Using Multi-Center MRA Datasets from Healthy Subjects. *Scientific data* **2019**, *6* (1), 1–8.

(10) de Vos, V.; Timmins, K. M. Automatic Cerebral Vessel Extraction in TOF-MRA Using Deep Learning. **2021**, 11.

(11) Hindenes, L. B.; Håberg, A. K.; Johnsen, L. H.; Mathiesen, E. B.; Robben, D.; Vangberg, T. R. Variations in the Circle of Willis in a Large Population Sample Using 3D TOF Angiography: The Tromsø Study. *PLOS ONE* **2020**, *15* (11), e0241373. https://doi.org/10.1371/journal.pone.0241373.

(12) Wijesinghe, P.; Steinbusch, H. W. M.; Shankar, S. K.; Yasha, T. C.; De Silva, K. R. D. Circle of Willis Abnormalities and Their Clinical Importance in Ageing Brains: A Cadaveric Anatomical and Pathological Study. *Journal of Chemical Neuroanatomy* **2020**, *106*, 101772. https://doi.org/10.1016/j.jchemneu.2020.101772.

(13) Timmins, K.; van der Schaaf, I.; Vos, I.; Ruigrok, Y.; Velthuis, B.; Kuijf, H. Deep Learning with Vessel Surface Meshes for Intracranial Aneurysm Detection. In *Medical Imaging 2022: Computer-Aided Diagnosis*; SPIE, 2022; Vol. 12033, pp 633–637.

(14) Danielsson, P.-E. Euclidean Distance Mapping. *Computer Graphics and Image Processing* **1980**, *14* (3), 227–248. https://doi.org/10.1016/0146-664X(80)90054-4.

(15) Klein, S.; Staring, M.; Murphy, K.; Viergever, M. A.; Pluim, J. P. W. Elastix: A Toolbox for Intensity-Based Medical Image Registration. *IEEE Transactions on Medical Imaging* **2010**, *29* (1), 196–205. https://doi.org/10.1109/TMI.2009.2035616.

APPENDIX

Parameter files for the registration of the pre-processed intensity atlas and TOF-MRA. The resulting transformation parameters are used to transform the radius, STD and probability atlas (changing final B-spline =1) (Section 2.2.1).

I) Affine transformation

```
(NumberOfResolutions 4)
(HowToCombineTransforms "Compose")
(AutomaticTransformInitialization "true")
(AutomaticScalesEstimation "true")
(AutomaticTransformInitializationMethod
"CenterOfGravity" )

(WriteTransformParametersEachIteration
"false")
(WriteResultImage "false")
(ResultImagePixelType "float")
(ResultImageFormat "nii.gz")
(CompressResultImage "true")
(WriteResultImageAfterEachResolution
"false")
(ShowExactMetricValue "false")

//Maximum number of iterations in each
resolution level:
(MaximumNumberOfIterations 1000)

//Number of grey level bins in each
resolution level:
(NumberOfHistogramBins 32 )
(FixedLimitRangeRatio 0.0)
(MovingLimitRangeRatio 0.0)
(FixedKernelBSplineOrder 3)
(MovingKernelBSplineOrder 3)

//Nr of spatial samples used to compute
the MI in each resolution level:
(ImageSampler "Random")
(NumberOfSpatialSamples 2000 )
(NewSamplesEveryIteration "true")
(CheckNumberOfSamples "true")
(MaximumNumberOfSamplingAttempts
10)

//Order of B-Spline interpolation in each
resolution level:
(BSplineInterpolationOrder 1)

//Order of B-Spline interpolation used for
applying the final deformation:
(FinalBSplineInterpolationOrder 0)
//Default pixel value for pixels that come
from outside the picture:
(DefaultPixelValue 0)

(MaximumStepLength 4.0)
```

II) B-spline

```
//_____ImageTypes_____________________
(FixedInternalImagePixelType "float")
(FixedImageDimension 3)
(MovingInternalImagePixelType "float")
(MovingImageDimension 3)

(ErodeMask "false" )
(FinalGridSpacingInPhysicalUnits 5.0 5.0
5.0)
(HowToCombineTransforms "Compose")

(WriteTransformParametersEachIteration
"false")
(WriteResultImage "true")
(ResultImagePixelType "float")
(ResultImageFormat "nii.gz")
(CompressResultImage "true")
(WriteResultImageAfterEachResolution
"false")
(ShowExactMetricValue "false")

(UseFastAndLowMemoryVersion "true")
(DefaultPixelValue 0)

//_____Similarity Metric_____________
(Metric
"AdvancedMattesMutualInformation")

//_____ Image Sampler ________________
(ImageSampler "RandomCoordinate")
(UseRandomSampleRegion "true")
(SampleRegionSize 50.0 50.0 50.0)
(NumberOfSpatialSamples 2000 )
(NewSamplesEveryIteration "true")
(CheckNumberOfSamples "true")
(MaximumNumberOfSamplingAttempts
10)

(Resampler "DefaultResampler")
(ResampleInterpolator
"FinalBSplineInterpolator")
(FixedImageBSplineInterpolationOrder 1 )

//_____ Interpolator (each resolut. level)___
(Interpolator "BSplineInterpolator")
(BSplineInterpolationOrder 5)

//_____ Final Interpolator _____________
(FinalBSplineInterpolationOrder 1)

//_____ Transform _____________________
(Transform "BSplineTransform")

//_____ Optimiser _____________________
(Optimizer "StandardGradientDescent")

//_____ Multi resolution_____________
(NumberOfResolutions 5)
(MaximumNumberOfIterations 2000 )
(Registration
"MultiResolutionRegistration")
(FixedImagePyramid
"FixedSmoothingImagePyramid")
(MovingImagePyramid
"MovingSmoothingImagePyramid")

//Nr of grey level bins in each resolution
level:
(NumberOfHistogramBins 32 )
(FixedLimitRangeRatio 0.0)
(MovingLimitRangeRatio 0.0)
(FixedKernelBSplineOrder 3)
(MovingKernelBSplineOrder 3)

//SP: Param_a in each resolution level. a_k
= a/(A+k+1)^alpha
(SP_a 10000.0 )

//SP: Param_A in each resolution level. a_k
= a/(A+k+1)^alpha
(SP_A 100.0 )

//SP: Param_alpha in each resolution level.
a_k = a/(A+k+1)^alpha
(SP_alpha 0.6 )
```